

Study of cytotoxic effect of photodynamically and sonodynamically activated sensitizers *in vitro*

K. Tomankova^a, H. Kolarova^{a,*}, P. Kolar^a, K. Kejlova^b, D. Jirova^b

^a Department of Medical Biophysics, Faculty of Medicine, Palacky University in Olomouc, Hnevotinska 3, 775 15 Olomouc, Czech Republic

^b National Institute of Public Health, Srobarova 48, 100 42 Prague, Czech Republic

ARTICLE INFO

Article history:

Received 31 October 2008

Accepted 6 July 2009

Available online 10 July 2009

Keywords:

Photodynamic therapy

Sonodynamic therapy

Antioxidant

Atomic force microscopy

ABSTRACT

High resolution imaging of biological structures and their changes induced by different agents such as drugs are commonly performed by confocal and electron microscopy. The past decade has witnessed an emersion of the atomic force microscopy (AFM) from solid-state physics into cell biology and even medical applications. For these reasons, we used this relatively new microscopic technique to study the morphology of cell lines.

We imaged the cells by atomic force microscopy before and after the photodynamic therapy (PDT) using the photosensitizer CIAIPcS₂. We also compared the impact of the photosensitizer in combination with silymarin antioxidant on cancer and non-cancer cell lines by measuring the kinetic production of reactive oxygen species (ROS). PDT was induced by LED source with total irradiation dose of 15 J cm⁻² and SDT was induced by therapeutic ultrasound with frequency of 1 MHz, intensity 2 W cm⁻² and time of exposition 10 min.

The results show ROS kinetic production within the cells during PDT, sonodynamic therapy (SDT) and modification of morphological features investigated by AFM. The combination of a sensitizer and the specific light source can lead to the loss of surface rigidity and eventually to dramatic changes of the cell shape, which we can study by AFM.

© 2009 Elsevier Ltd. All rights reserved.

1. Introduction

Photodynamic therapy (PDT) of malignancies is a widely used technique based on photochemical sensitization induced by a combination of tumour-localizing photosensitizer and visible light (Nakaseko et al., 2003) and oxygen. By treatment of the irradiation of visible light with appropriate wavelength, the photosensitizer can drive molecular oxygen into excited triplet state transferring energy into ground state molecular oxygen which produces singlet molecular oxygen. Activated singlet oxygen, or reactive oxygen species (ROS) in general, plays an important role in cytotoxic effects on tumor tissues. Photodynamic therapy of the tumour cells is sometimes associated with rapid initiation of apoptosis, a mode of cell death that results in a distinct pattern of cellular and DNA fragmentation.

Abbreviation: PDT, photodynamic therapy; SDT, sonodynamic therapy; ROS, reactive oxygen species; AFM, atomic force microscopy; LED, light emitting diode; UV, ultraviolet; DNA, deoxyribonucleotic acid; DSU, disc scanning unit; MTT, moving target tracking; FWHM, full width half maximum; PLL, poly-L-lysine; GA, glutaraldehyde.

* Corresponding author. Tel.: +420 585 632 101; fax: +420 585 632 167.

E-mail address: hana.kolarova@upol.cz (H. Kolarova).

Sonodynamic therapy is a newer concept, which refers to the ability of ultrasound to evoke cytotoxic effect on cell lines (Kessel et al., 1996). The cytotoxicity of SDT can be enhanced by the presence of sonosensitizing drugs. Ultrasound can be focused onto a small region of tumour to activate the sonosensitizing drug and, in contrast with PDT, can penetrate deeply into the tissue (Yumita and Umemura, 2003). Kessel et al., suppose that cytotoxic effect of SDT is mediated largely by inertial cavitation (Kessel et al., 1994). Inertial cavitation is a process where a gas bubble created in a liquid by ultrasound rapidly collapses, producing a shock wave with an intensive heat release (of several thousand degrees Kelvin) (Worthington et al., 1997). The water molecules surrounding the cavitation decompose into their ·H and ·OH constituents (water pyrolysis), which either recombine, forming H₂O, H₂O₂, and H₂, directly oxidize or reduce solute molecules, sonosensitizing drugs or the cell biomolecules (Suslick, 1990). It is expected that the affinity of the agent to tumour and its ability to generate singlet oxygen is very important in understanding the mechanism of SDT (Sadzuka et al., 2006).

In the past two decades there has been an explosive interest in the role of oxygen-free radicals more generally known as reactive oxygen species (ROS) in experimental and clinical medicine. ROS are generated during irradiation by UV light, X-rays and by gam-

ma-rays. ROS are products of metal-catalyzed reactions, they are present as pollutants in the atmosphere, they are induced by neutrophils and macrophages during inflammation they may be generated as by-products of mitochondria-catalyzed electron transport reactions and other mechanisms (Valko et al., 2006). The reactive oxygen species are formed and degraded by all aerobic organisms, leading to either physiological concentrations required for normal cell function or in excessive quantities, resulting in the state called oxidative stress. As the term ROS implies, intracellular production of the oxygen intermediates threatens the integrity of various biomolecules including proteins, lipids as well as lipoproteins involved in arteriosclerosis and DNA (Nordberg and Arnér, 2001).

Oxidative stress is also proposed to be involved in the process of aging by inducing damage to mitochondrial DNA and by other mechanisms (Nordberg and Arnér, 2001). Free radicals can be defined as molecules or molecular fragments containing one or more unpaired electrons. The presence of unpaired electrons usually confers considerable degree of reactivity upon a free radical. The derived oxygen radicals derived from oxygen represent the most important class of such species generated in living systems.

In normal physiology, there is a dynamic equilibrium between ROS activity and antioxidant defense capacity, however, when the equilibrium shifts in favour of ROS, either by a reduction in antioxidant defenses or an increase in ROS production or activity, oxidative stress occurs (Chapple and Matthews, 2007). A balance between oxidant and antioxidant intracellular systems is hence vital for cell function, regulation and adaptation to diverse growth conditions (Nordberg and Arnér, 2001).

Antioxidants are substances which offer protection against lipid oxidation, react and interfere with free radicals, reduce oxidative stress, and stop low-density lipoproteins from being oxidized (Chapple and Matthews, 2007). The effect of ROS is balanced by the antioxidant action of non-enzymatic antioxidants, as well as by antioxidant enzymes. Such antioxidant defences are extremely important as they represent direct removal of free radicals (pro-oxidants), thus providing maximal protection for biological sites. A good antioxidant should: specially quench free radicals, chelate redox metals, interact with other (regenerate) antioxidants within the antioxidant network, and have a positive effect on gene expression (Valko et al., 2006). Silymarin, an extract from milk thistle plant (*Silybum marianum*) is a powerful natural protector of the cellular membrane due to its antioxidantizing and anti-free radical power. For this reason it is used in all kinds of anti-aging treatments and cancer prevention (Ramasamy and Agarwal, 2008).

We are able to study the morphological changes in cells caused by oxidative stress using different microscopic methods. One of the methods enabling the 3D imaging of the cell morphology is the atomic force microscopy (AFM). Imaging of the cell surface was formerly considered as an important biological application of the scanning probe microscopy and more particularly the atomic force microscopy. At present, the atomic force microscopy is extensively used in the wide range of bio-disciplines to image surfaces on scales from micrometer to nanometer with the objective to visualize and properly characterize surface textures and shapes. The biological material is scanned in non-contact or semi-contact mode allowing the visualization of the delicate samples in air and other surroundings (Vie et al., 2000; Lee and Mash-Lee, 2004). The study of changes in the membrane surface topography in living or dead cells may open a new field of application for atomic force microscopy (Vie et al., 2000). Differences in relief of the cell surface give us information on the cell damage and different components of the cell wall. The aim of this study was to test the influence of sensitizer, ultrasound and antioxidant in combination with visible light and with the appropriate wavelength on tumor cell line and to verify the influence of these drugs and treatments on non-tumorous cell line. For this work, cell line B16FO (mouse melanoma cell) a

DV41 (mouse fibroblast cell) were selected and PDT, SDT and chemo-protective consequence of silymarin, as nature drugs, were applied and effects were verified. These cell lines were chosen with regard to PDT in clinical application, because skin and skin tumors are well accessible to visible light, which is necessary to induce photodynamic treatments. Nowadays nanotechnology penetrates all domains of biological, biophysical and biomedical studies. Our article aims to help implement the biological application of AFM in the studies of cell damaging by the means of new microscopical methods among which AFM inherently belongs. Another aims of this study were to picture cancer and non-cancer cells in air by AFM before and after PDT, to examine the cytotoxic effect in ROS production and to study the influence of silymarin on ROS production and consequent cytotoxic effect.

2. Materials and methods

2.1. Materials and instruments

Cell lines B16FO (mouse melanoma cells) and NIH3T3 (mouse fibroblast cells) were used as a biological material. The chemicals used included Dulbecco's Modified Eagle Medium (DMEM), sensitizer ClAlPcS₂ (prepared by Jan Rakusan at the Research Institute for Organic Syntheses in Rybitvi, Czech Republic), poly-L-lysine (PLL, Sigma–Aldrich), glutaraldehyde (GA, Sigma–Aldrich), 5-(and-6)-chloromethyl-2',7'-dichlorodihydrofluorescein diacetate (CM-H₂DCFDA, Invitrogen Co., USA), 3-(4,5-dimethyl-2-thiazolyl)-2,5-diphenyl-2H-tetrazolium bromide (MTT, Sigma–Aldrich), Annexin FITC Apoptosis Detection Kit (Sigma Aldrich), dimethyl sulfoxide (DMSO, Sigma–Aldrich), antioxidant silymarin (Provital Group). Measurements were carried out on AFM Ntegra Aura (NT-MDT, Russia), multi-detection microplate reader Synergy HT (BioTek, USA), therapeutic ultrasound (BTL 4000, USA), LED diodes L53SRC-F, maximum 660 nm, FWHM 24 nm (Kingbright Corporation, Taiwan), transmission microscope Olympus IX81 with DSU unit (Olympus, Japan). We used the Thermanox® sterile plastic microscope slides as substrates for cells and 35 mm Petri dishes for cultivation of the cell lines.

2.2. Photodynamic and sonodynamic therapy

3.3×10^5 NIH3T3 or B16FO cells were seeded into the 35 mm Petri dishes containing 2 ml of cultivation medium (DMEM) – with photosensitizer ClAlPcS₂ added in concentrations 0 (control), 0.5, 1, 5, 10, 50 and 100 μM . The cells were incubated in a thermobox at 37 °C, 5% CO₂ atmosphere for 24 h. Before starting the experiments we replaced DMEM by PBS containing 5 mM glucose and added 20 μl of 500 mM CM-H₂DCFDA (dissolved in DMSO). One dish was used as control (cells in the absence of sensitizer), one dish was used as negative control (cells in the absence of sensitizer and irradiated with a dose 15 J cm⁻²). Other dishes, i.e. cells in the presence of 0.5, 1, 5, 10, 50 and 100 μM ClAlPcS₂, were irradiated with total dose of 15 J cm⁻². For the irradiation, we used light emitting diodes with the emission wavelength maximum at 660 nm, FWHM 25 nm. The light intensity was set to 0.1 mW.cm⁻² (internal irradiator) for kinetic measurements and 12 mW cm⁻² for subsequent irradiation up to the total dose of 15 J cm⁻² using external LED irradiator. The arrangement of the experiments was following: CM-H₂DCFDA incubation for 30 min, kinetic measurement of ROS production during PDT, irradiation up to the total dose of 15 J cm⁻², and measurement of total ROS production. In experiments with silymarin, we added 15 $\mu\text{l ml}^{-1}$ (15 $\mu\text{g ml}^{-1}$) of the antioxidant solved in water, before starting the kinetic measurement of ROS production. In experiments with SDT, we performed ultrasound irradiation before starting the kinetic measurement of

ROS production. Parameters of ultrasound exposition were following: frequency 1 MHz, intensity 2 W.cm^{-2} and time of exposition 10 min. After these treatments, cells were cultivated for the next 24 h under the same conditions in fresh DMEM medium.

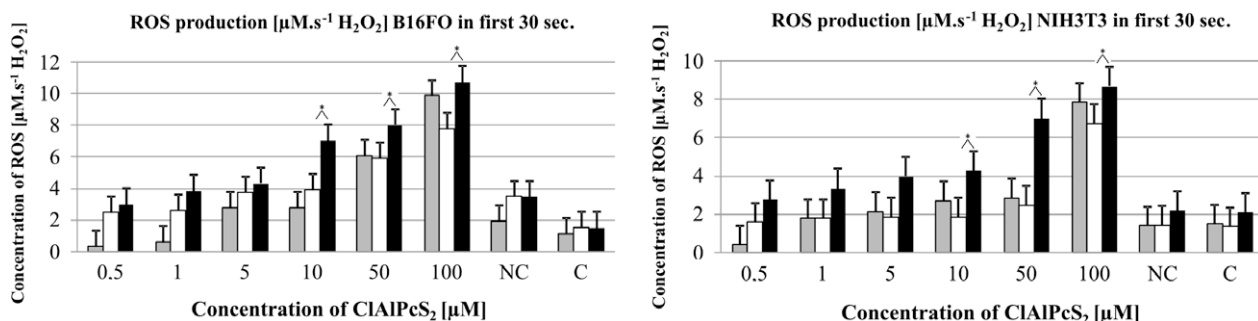
2.3. Measurement of ROS production

ROS were generated due to PDT and SDT influence. We determined ROS production during PDT using CM-H₂DCFDA and microplate reader Synergy HT. Excitation wavelength of 485 nm and emission wavelength of 548 nm were used. The time course of

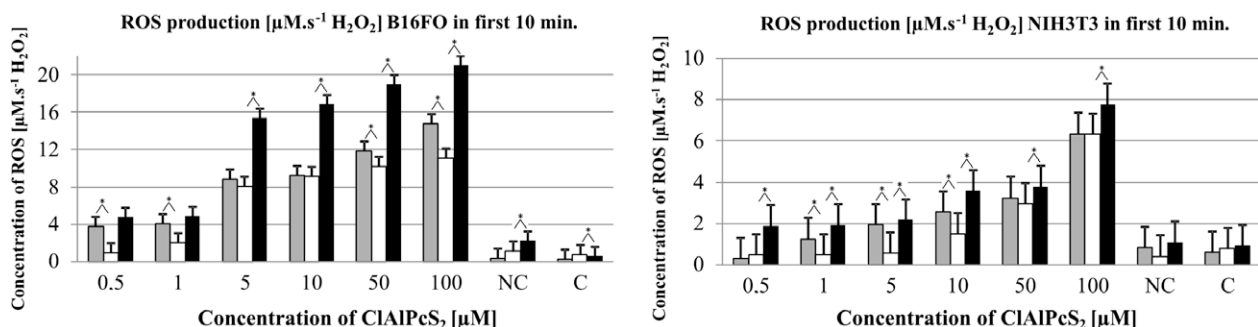
ROS generation was recorded for 10 min at the light intensity of 0.1 mW cm^{-2} produced by LEDs with internal irradiator inserted into the microplate reader. The total ROS production was measured after termination a 20-min irradiation with microplate reader and external irradiator inserted to the thermobox at a higher intensity of 12 mW cm^{-2} with a final dose of 15 J cm^{-2} .

2.4. Cancer cell cytotoxicity assay

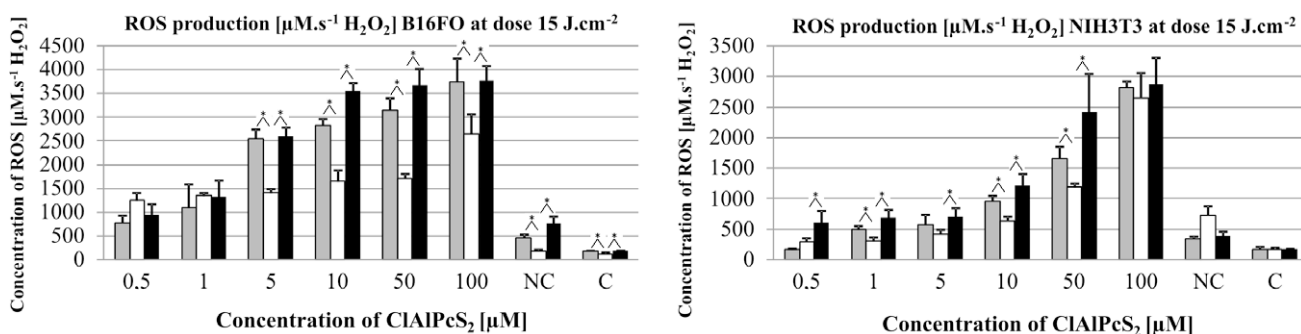
The cytotoxic effect of the sensitizer CIAIPcS₂ in combination with irradiation, ultrasound exposition and the protective effect



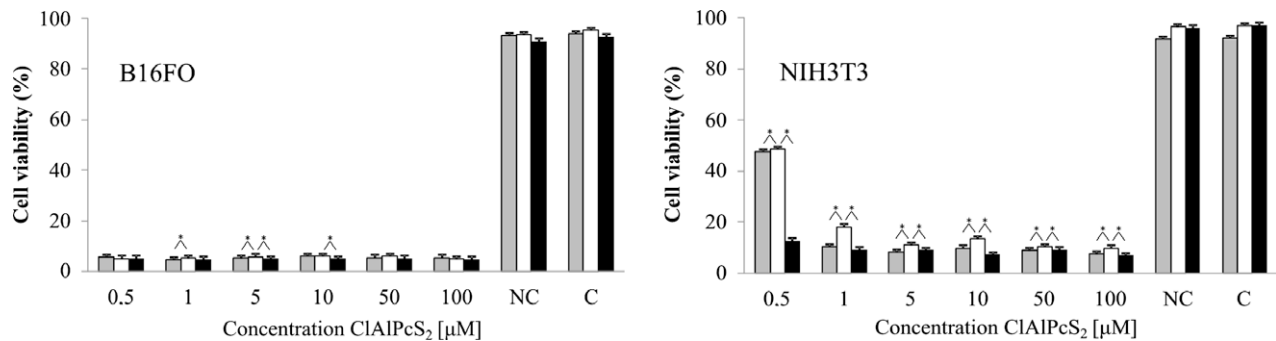
Graph 1. Kinetic production of ROS at the first 30 s in B16FO and NIH3T3 cell line in $\mu\text{M s}^{-1} \text{H}_2\text{O}_2$ per 10^4 B16FO and NIH3T3 with CIAIPcS₂ sensitizer at concentration of 0.5, 1, 5, 10, 50, 100 μM and during PDT (grey columns) and comparison at the same concentrations with the addition of silymarin (white columns) and with SDT (black columns). C = control without sensitizer and without light irradiation (grey column) with silymarin (white column) and with ultrasound exposition (black column), NC = negative control without sensitizer and with light irradiation (grey column) with silymarin (white column) and with ultrasound exposition (black column).



Graph 2. Kinetic production of ROS at the first 10 min in B16FO and NIH3T3 cell line in $\mu\text{M s}^{-1} \text{H}_2\text{O}_2$ per 10^4 B16FO and NIH3T3 with CIAIPcS₂ sensitizer at concentration of 0.5, 1, 5, 10, 50, 100 μM and during PDT (grey columns) and comparison at the same concentrations with the addition of silymarin (white columns) and with SDT (black columns). C = control without sensitizer and without light irradiation (grey column) with silymarin (white column) and with ultrasound exposition (black column), NC = negative control without sensitizer and with light irradiation (grey column) with silymarin (white column) and with ultrasound exposition (black column).



Graph 3. Kinetic production of ROS at the light dose 15 J cm^{-2} in B16FO and NIH3T3 cell line in $\mu\text{M s}^{-1} \text{H}_2\text{O}_2$ per 10^4 B16FO and NIH3T3 with CIAIPcS₂ sensitizer at concentration of 0.5, 1, 5, 10, 50, 100 μM and during PDT (grey columns) and comparison at the same concentrations with the addition of silymarin (white columns) and with SDT (black columns). C = control without sensitizer and without light irradiation (grey column) with silymarin (white column) and with ultrasound exposition (black column), NC = negative control without sensitizer and with light irradiation (grey column) with silymarin (white column) and with ultrasound exposition (black column).



Graph 4. Cell viability of the B16FO and NIH3T3 cell line 24 h after PDT with CIAIPcS₂ sensitizer at concentration of 0.5, 1, 5, 10, 50, 100 µM and with light dose 15 J cm⁻² (grey columns) and comparison at the same concentrations with the addition of silymarin (white columns) and with SDT (black columns). C = control without sensitizer and without light irradiation (grey column) with silymarin (white column) and with ultrasound exposition (black column), NC = negative control without sensitizer and with light irradiation (grey column) with silymarin (white column) and with ultrasound exposition (black column).

of silymarin, on B16FO and NIH3T3 cells was determined using the MTT assay. After treatment, cells were incubated at 37 °C and 5% CO₂ for 24 h in fresh DMEM. Before starting the experiments we replaced DMEM by PBS containing 5 mM glucose, added 222 µl 20 mM MTT (dissolved in PBS) and incubated the cells for 3 h at 37 °C and 5% CO₂. The MTT solution was carefully removed and

1 ml DMSO we added in order to solubilize the violet formazan crystals. The absorbance of the resulting solution was measured in 96-well microplate reader Synergy HT at 570 nm and 690 nm. The cell viability of the samples was determined as percentage of control cell viability (100 × average of test group/average of control group).

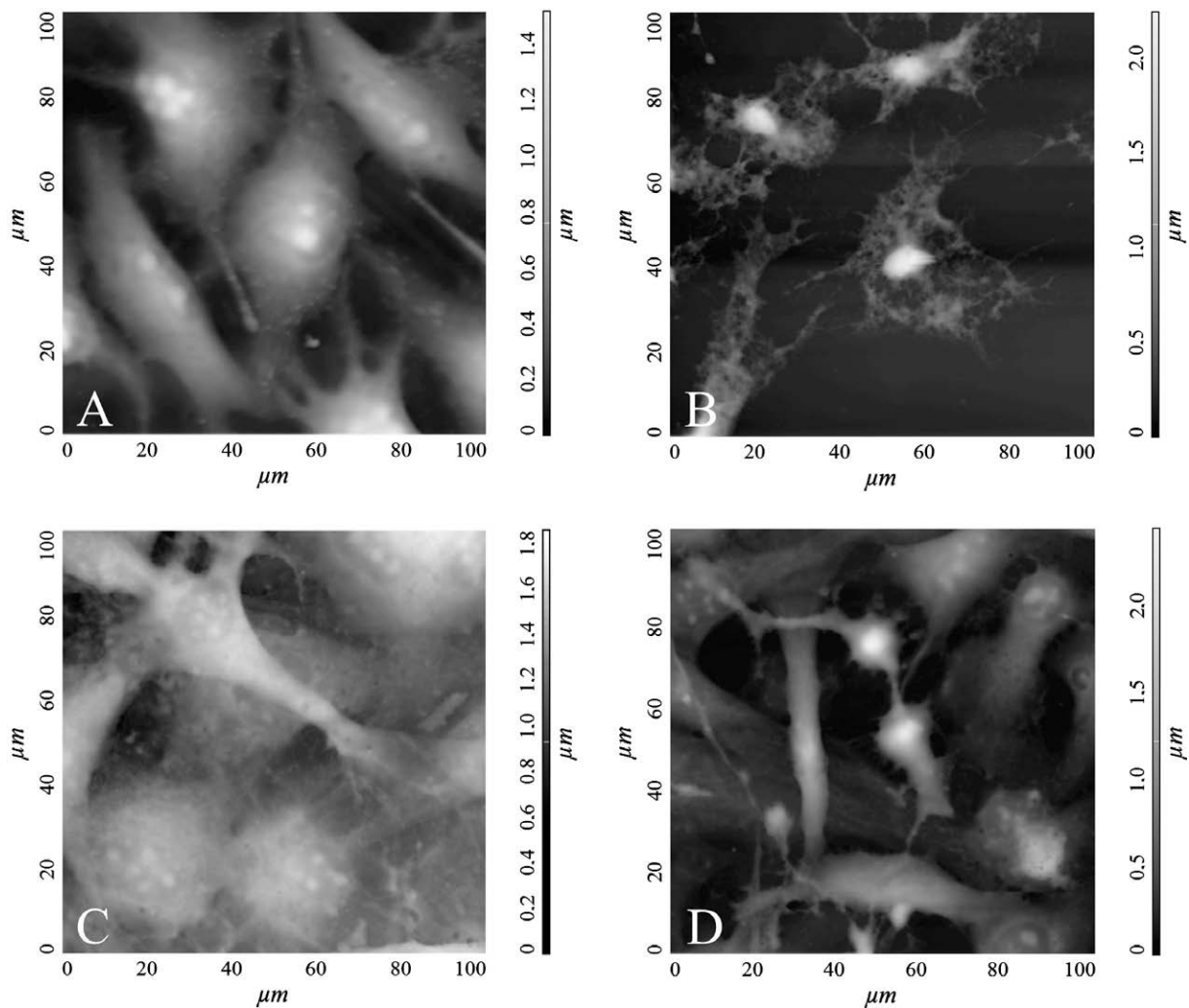


Fig. 1. Non-irradiated cells of the B16FO cell line, is shown in A, NIH3T3 is shown in C. In Fig. 1B cell line B16FO and in D NIH3T3 after PDT with concentration 100 µM of CIAIPcS₂ and light dose are shown 15 J·cm⁻². The image was obtained in a semi-contact topography mode (size 100 × 100 µm, resolution 256 × 256 pixels, and scan rate 80 µm s⁻¹). The height of the cell is expressed in colour scale 0 (dark fields) – 1.5 µm (light fields) on A, 0–2.2 µm on B, 0–1.9 µm on C and 0–2.3 µm on D.

2.5. AFM and sample preparation

Thermanox[®] poly-L-lysine treated plastic discs were used for the cell imaging. Plastic discs were incubated in 0.01% PLL overnight. After incubation, the discs were rinsed in deionized water for 1 min, moved to sterile 35 mm Petri dishes and stored at 4 °C. 2×10^5 of B16FO or NIH3T3 cells were seeded into the 35 mm Petri dishes containing the pre-treated Thermanox[®] discs, 2 ml of cultivation medium (DMEM), and photosensitizer CIAIPcS₂ in concentrations 0 (control) and 100 μmol. Then the samples were kept for 24 h in a thermobox at 37 °C and 5% CO₂. PDT was performed with light dose of 15 J cm⁻². Subsequently, the cells were gently fixated with glutaraldehyde (final concentration of GA was 0.5% in DMEM) for 20 min (Riethmuller et al., 2007). The imaging was performed at a high dry level. Samples were rinsed by deionized water before drying, ensuring removal of the crystals. We imaged the cell line before and after the photodynamic therapy by a dry scanner at size of 100 × 100 μm. We used a NSG10 tip, with a resonant frequency of 190–325 kHz and a force constant of 5.5–22.5 N m⁻¹. All images were processed by Nova software.

2.6. Fluorescent microscopy and annexin viability test

Cell viability and morphological changes after PDT were visualized by Olympus IX80 microscope with DSU unit. The measurement was carried out in 96-well plate. After treatment, cells were incubated at 37 °C and 5% CO₂ for 24 h in fresh DMEM. Before starting the measurements we replaced DMEM by 200 μl PBS con-

taining 5 mM glucose, added 5 μl of propidium iodide and 2.5 μl of annexin and incubated at 37 °C and 5% CO₂ for 30 min. Images were recorded by CCD camera and Cell^R software. Image Analysis Olympus Micro Image software was used for count necrotic and apoptotic cell. These cells were encompassed to 1 000 cell.

2.7. Statistic analysis

All data were presented as ± mean SD of four independent experiments. The statistical significance was determined using Kruskal–Wallis Test and Mann–Whitney U-Test. The results were process at SPSS v. 15 (SPSS Inc. Chicago, USA). $P \leq 0.05$ was considered statistically significant.

3. Results

Our results revealed changes of B16FO and NIH3T3 cells after induction of PDT induced by red light at the dose of 15 J cm⁻² in the presence of 0 (control), 0.5, 1, 5, 10, 50 and 100 μM CIAIPcS₂. We measured kinetic production of ROS during photodynamic therapy and we detected final ROS production at dose 15 J cm⁻². The results of kinetic production measured during the first 30 s, 10 min as well as the final production of ROS, are summarized in Graphs 1–3. Kinetic production increased with rising concentrations of the photosensitizer and decreased with time of kinetic measurements in NIH3T3 cell line. On the other hand, in cell line B16FO the kinetic production increased with rising concentrations of the photosensitizer and with time of kinetic measurements too.

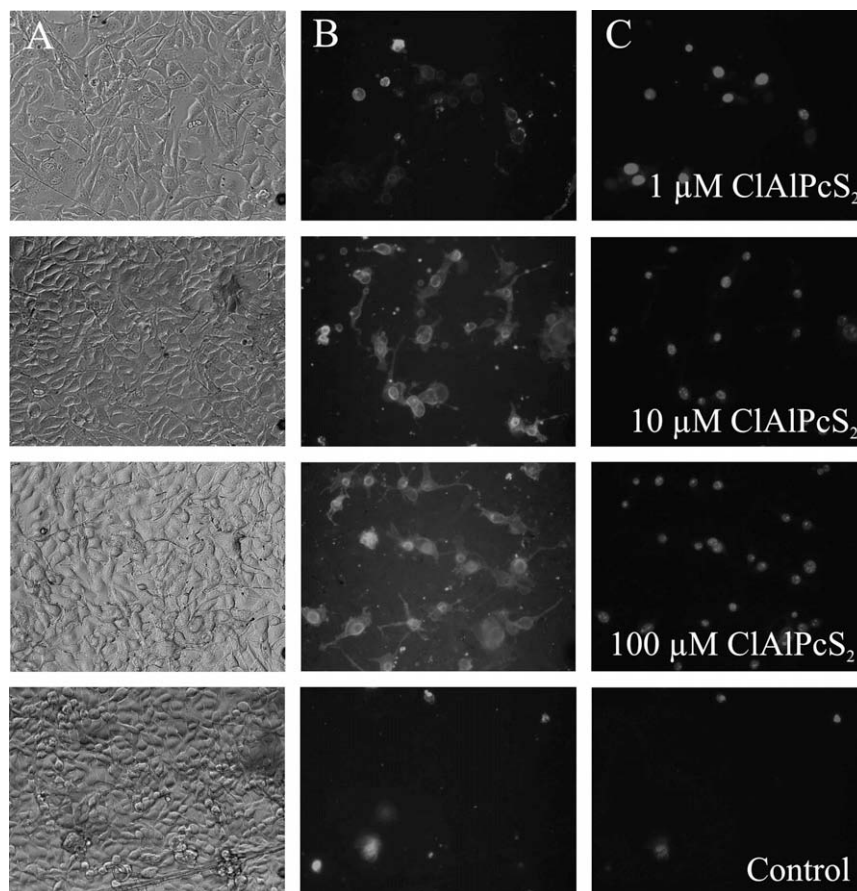


Fig. 2. B16FO cell line before PDT (control) and after PDT (columns A, B, C) with concentration of CIAIPcS₂ 1, 10, 100 μM. Images in column A were created using transmitted light, in column B were created by fluorescence for imaging of apoptosis by annexin, and at column C were created by fluorescence for imaging of necrosis by propidium iodide.

In **Graphs 1 and 2**, we show kinetic production of ROS under the same conditions with additional ultrasound exposition and with the addition of silymarin ($15 \mu\text{g ml}^{-1}$). These results show that kinetics (see **Graphs 1 and 2**) and final production (see **Graph 3**) of ROS are decreased by addition of silymarin mostly in higher concentrations of sensitizer. The ultrasound exposition enhanced the production of ROS. The increase in the production of ROS with concentration of CIAIPcS₂ was retained. Cell viability of the B16FO and NIH3T3 cell lines 24 h after PDT, SDT and addition of silymarin with CIAIPcS₂ sensitizer is shown in **Graph 4**. Viability of the NIH3T3 cells is higher after addition of silymarin as statistic analysis revealed. The increase of cell line B16FO viability is not so evident. However, it is clear, that the lower ROS production after treatments leads to higher viability of the cells.

Microscopic study (**Fig. 1**) shows morphological changes in the cell general culture before and after photodynamic treatment. **Fig. 1A** presents undamaged control mouse melanoma cell line B16FO without irradiation; **Fig. 1B** shows photodamaged B16FO cells after PDT with CIAIPcS₂ at concentration 100 μM and dose of light irradiation 15 J cm^{-2} . The non-tumorous cell line of mouse fibroblasts NIH3T3 before PDT is demonstrated on **Fig. 1C** and the cell line NIH3T3 after PDT is recorded in **Fig. 1D**. The live B16FO and NIH3T3 cell lines are spread in a monolayer on the substrate with the cytoplasm of the individual cells approaching each other. On the other hand, the photodynamically treated cells undergo cell death. The images were obtained in a semi-contact topography mode (size $100 \times 100 \mu\text{m}$, resolution 256×256 pixels, scan rate $80 \mu\text{m s}^{-1}$). The height of the cells is expressed using a colour scale.

The reproducible high resolution topographic AFM images were obtained in air with glutaraldehyde fixation in semi-contact mode.

In order to improve the adhesion properties of the cells the Thermanox[®] plastic dishes were modified by 0.01% poly-L-lysine. In another microscopic study we detected the state of the cell lines after PDT by annexin viability kit (see **Figs. 2 and 3**) at concentrations 0 (control), 1, 10, 100 μM of CIAIPcS₂. In columns A we can see light microscopic images of untreated cells, in columns B we recorded the quantity of apoptotic cells using annexin, and in columns C we recorded the numbers of necrotic cells using propidium iodide. Image analysis revealed the number of necrotic and apoptotic cells from 1000 cells in samples. The number of apoptotic cells in B16FO cell line: in concentration 1 μM of CIAIPcS₂ – 4.7%, in concentration 10 μM of CIAIPcS₂ – 8.8%, in concentration 100 μM of CIAIPcS₂ – 10% in control sample 3.1%. The necrotic cells were: 5.2%, 8.2%, 10.8% and 2.1% in the same order of sensitizer concentration. The number of apoptotic cells in cell line NIH3T3: in concentration 1 μM of CIAIPcS₂ – 2.4%, in concentration 10 μM of CIAIPcS₂ – 7.1%, in concentration 100 μM of CIAIPcS₂ – 5.3% in control sample 2.4%. The necrotic cells were: 0.7%, 3%, 9.4% and 1.6% in the same order of sensitizer concentration.

4. Discussion

Silymarin is the active compound of the *Silybum marianum* plant. It is not a pure chemical compound, but a mixture of several structural isomers from the flavanoligane group. This mixture includes three major isomers (silibine, silicristine and silidianine)

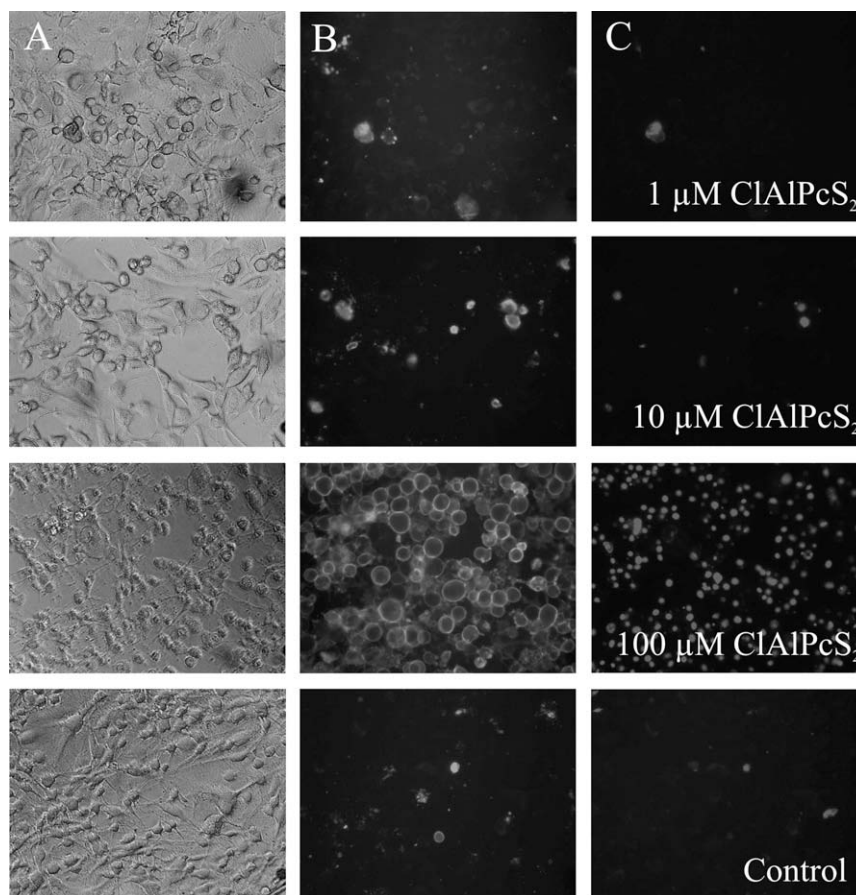


Fig. 3. NIH3T3 cell line before PDT (control) and after PDT (columns A, B, C) with concentration of CIAIPcS₂ 1, 10, 100 μM . Images in column A were created using transmitted light, in column B were created by fluorescence for imaging of apoptosis by annexin, and at column C were created by fluorescence for imaging of necrosis by propidium iodide.

and two more which are only contained in a small proportion (isosilibine and isosilicristine). These five substances are flavanol derivatives composed by taxifolin and coniferyl alcohol. The changes in production of ROS within treatments (a comparison between PDT, SDT and addition of silymarin) are evident at higher concentrations of the sensitizer. In lower values of concentrations protective effect is not so prominent. The added silymarin acts as protection against free radicals, as it decreases the production of ROS (see *Graphs 1–3*). On the other hand, ultrasound treatment increases the production of ROS. These processes are marked particularly in higher concentrations of CIAIPcS₂. The sequence of the treatments affects the production of ROS. The highest production of ROS is acquired by application of SDT after PDT (Tomankova et al., 2008). The decreased production of ROS (for example due to antioxidants) leads to the increase of cell viability, while the increase of ROS production by ultrasound exposition leads to decreased cell viability (see *Graphs 3 and 4*). These effect are evident in all concentrations of the sensitizer, principally in cell line NIH3T3.

In summary, the tumorous cell line B16FO has higher sensitivity to PDT, however, the non-tumorous cell line NIH3T3 shows bigger differences between individual treatments, i.e. combination of PDT with SDT of addition of silymarin, which consequently is shown mostly in cell viability (see *Graph 4*). On the basis of these results, we may suggest, that antioxidant can protect non-tumorous cell against photodynamic therapy.

Common optical microscopy is unable to provide high resolution and 3D imaging, therefore we imaged the cells using atomic force microscopy. The drying method used reflects morphology of the cells in the stage closely before drying. The live undamaged cells treated by this procedure have elongated shape in comparison with photodynamically damaged cells. In general, the shape of the cells depends on the type and also on the state of the cell; for example, dead cells are characterized by circular or elliptic shape in comparison with the oblong shape of live cells. Although the cell surface structure has been studied extensively by other microscopy techniques, in our opinion the possibility offered by AFM investigation appears unique and interesting. The height of the non-treated cells is smaller than the height of the cell after PDT due to different adherent properties (Boudreault and Grygorczyk, 2004). In our study, non-tumorous NIH3T3 cells appear to be less damaged than tumorous B16FO cells after PDT. A tight fixation of cells onto substrate is a necessary condition for high-resolution imaging. For this purpose, substrates can be modified by different biological (gelatin coated) (Doktycz et al., 2003) or polymeric (Poly-L-lysine treated) (Richert et al., 2004) materials. In order to acquire high resolved cell image in air, chemical fixation onto Thermanox[®] plastic discs is necessary. In this case the most widely used ingredient is glutaraldehyde (GA) (Hutter et al., 2005). The effect of the drying procedure may cause a certain degree of flattening in the nanostructure of the sample and this was taken into account during interpretation of the results.

Detection by fluorescent microscope revealed, that the numbers of apoptotic cells were higher than the numbers of necrotic cells, depending on the concentration of the sensitizer. In lower concentration of sensitizer predominate the apoptosis, however, in high

concentration, for example 100 μM of CIAIPcS₂, the number of necrosis cells is higher, than number of apoptotic cells, which may be caused by deficiency of media nutrient components and own cytotoxicity of high sensitizer concentration because this effect is similar in non-apoptotic cells (see *Figs. 2 and 3*).

Acknowledgements

This work was supported by the Grant Project MSM 6198959216 and IGA NS 9648-4 and 21211152. Thanks to Jana Zapletalova to statistic analysis.

References

- Boudreault, F., Grygorczyk, R., 2004. Evaluation of rapid volume changes of substrate-adherent cells by conventional microscopy 3D imaging. *Journal of Microscopy* 215, 302–312.
- Chapple, I.L.C., Matthews, J.B., 2007. The role of reactive oxygen and antioxidant species in periodontal tissue destruction. *Periodontology* 2000 (43), 160–232.
- Doktycz, M.J., Sullivan, C.J., Hoyt, P.R., Pelletier, D.A., Wu, S., Allison, D.P., 2003. AFM imaging of bacteria in liquid media immobilized on gelatin coated mica surfaces. *Ultramicroscopy* 97, 209–216.
- Hutter, J.L., Cen, J., Wan, W.K., Uniyals, S., Leabu, M., Chan, M.C., 2005. Atomic force microscopy investigation of the dependence of cellular elastic moduli of glutaraldehyde fixation. *Journal of Microscopy* 219, 61–68.
- Kessel, D., Jeffers, R., Fowlkes, J.B., Cain, C., 1994. Porphyrin-induced enhancement of ultrasound cytotoxicity. *International Journal of Radiation Biology* 66, 221–228.
- Kessel, D., Jeffers, R., Fowlkes, J.B., Cain, C., 1996. Effects of sonodynamic and photodynamic treatment on cellular thiol levels. *Journal of Photochemistry and Photobiology B* 32, 103–106.
- Lee, J.W.M., Mash-Lee, N., 2004. A nano-view of West Nile virus-induced cellular changes during infection. *Journal of Nanobiotechnology* 2. doi:10.1186/1477-3155-2-6.
- Nakaseko, H., Kobazashi, M., Akita, Z., Tamada, Y., Matsumoto, Y., 2003. Histological changes and involvement of apoptosis after photodynamic therapy for actinic keratoses. *British Journal of Dermatology* 148, 122–127.
- Nordberg, J., Arnér, S.J., 2001. Reactive oxygen species, antioxidants and the mammalian thioredoxin system. *Free Radical Biology and Medicine* 31, 1287–1312.
- Ramasamy, K., Agarwal, R., 2008. Multitargeted therapy of cancer by Silymarin. *Cancer Letters* 269, 352–362.
- Richert, L., Arntz, Y., Schaaf, P., Voegel, J.C., Picart, C., 2004. PH dependent growth of poly(L-lysine)/poly(L-glutamic) acid multilayer films and their cell adhesion properties. *Surface Science* 570, 13–29.
- Riethmuller, C., Schaffer, T.E., Kienberger, F., Stracke, W., Oberleithner, H., 2007. Vacuolar structures can be identified by AFM elasticity mapping. *Ultramicroscopy* 107, 895–901.
- Sadzuka, Y., Tokutomi, K., Iwasaki, F., Sugiyama, I., Hirano, T., Konno, H., Oku, N., Sonobe, T., 2006. The phototoxicity of photofrin was enhanced by PEGylated liposome in vitro. *Cancer Letters* 241, 42–48.
- Suslick, K.S., 1990. Sonochemistry. *Science* 247, 1439–1445.
- Tomankova, K., Kolarova, H., Bajgar, R., 2008. Study of photodynamic and sonodynamic effect on A549 cell line by AFM and measurement of ROS production. *Physica Status Solidi A* 205, 1472–1477.
- Valko, M., Rhodes, C.J., Monocol, J., Izakovic, M., Mazur, M., 2006. Free radicals, metals and antioxidants in oxidative stress-induced cancer. *Chemico-Biological Interactions* 160, 1–40.
- Vie, V., Giocondi, M.C., Lesniewska, E., Finot, E., Goudonnet, J.P., Le Grimellec, C., 2000. Tapping-mode atomic force microscopy on intact cells: optimal adjustment of tapping conditions by using the deflection signal. *Ultramicroscopy* 82, 279–288.
- Wortington, A.E., Thompson, J., Rauth, A.M., Hunt, J.W., 1997. Mechanism of ultrasound enhanced porphyrin cytotoxicity. Part I: a search for free radical effects. *Ultrasound in Medicine and Biology* 23, 1095–1105.
- Yumita, N., Umemura, S., 2003. Sonodynamic therapy with photofrin II on AH130 solid tumor. Pharmacokinetics, tissue distribution and sonodynamic antitumoral efficacy of photofrin II. *Cancer Chemotherapy and Pharmacology* 51, 174–178.